

# Controlling Cherenkov angles with resonance transition radiation

Xiao Lin<sup>1,2</sup>, Sajan Easo<sup>3\*</sup>, Yichen Shen<sup>4</sup>, Hongsheng Chen<sup>1</sup>, Baile Zhang<sup>2,5</sup>,  
John D. Joannopoulos<sup>4</sup>, Marin Soljačić<sup>4</sup> and Ido Kaminer<sup>6</sup>

**Cherenkov radiation provides a valuable way to identify high-energy particles in a wide momentum range, through the relation between the particle velocity and the Cherenkov angle. However, since the Cherenkov angle depends only on the material's permittivity, the material unavoidably sets a fundamental limit to the momentum coverage and sensitivity of Cherenkov detectors. For example, ring-imaging Cherenkov detectors must employ materials transparent to the frequency of interest as well as possessing permittivities close to unity to identify particles in the multi-gigaelectronvolt range, and thus are often limited to large gas chambers. It would be extremely important, albeit challenging, to lift this fundamental limit and control Cherenkov angles at will. Here we propose a new mechanism that uses the constructive interference of resonance transition radiation from photonic crystals to generate both forward and backward effective Cherenkov radiation. This mechanism can control the radiation angles in a flexible way with high sensitivity to any desired range of velocities. Photonic crystals thus overcome the material limit for Cherenkov detectors, enabling the use of transparent materials with arbitrary values of permittivity, and provide a promising versatile platform well suited for identification of particles at high energy with enhanced sensitivity.**

The relation between the angle of Cherenkov radiation cones (denoted as the Cherenkov angle  $\theta$  below)<sup>1,2</sup> and the velocity  $v$  of charged particles is of fundamental importance to many applications<sup>3–6</sup>. For example, this determines the sensitivity of different types of Cherenkov detector such as the ring-imaging Cherenkov detectors<sup>7,8</sup> for particle identification.

However, the relation between the Cherenkov angle and the particle velocity is inherently limited by the material in which the Cherenkov radiation is emitted. This unavoidably sets a strict limit on the design of Cherenkov detectors. For conventional Cherenkov radiation generated in a non-magnetic material, when the particle velocity is known, the Cherenkov angle relies only on the material's relative permittivity  $\epsilon_r$  (which determines the refractive index  $n = \sqrt{\epsilon_r}$ ) through the formula  $\cos\theta = (n\beta)^{-1}$ , where  $\beta = \frac{v}{c}$  and  $c$  is the speed of light in free space. Regular transparent dielectrics are not suitable for conventional Cherenkov detectors. This is because these materials have a relative permittivity far above unity and the Cherenkov angle would saturate to a value independent of the particle velocity. As an example, quartz has a relative permittivity of around 2, limiting the useful momentum range to below 3.5 GeV/c (and even that requires using water instead of air to out-couple the light)<sup>9</sup>. Large volumes of gas radiators with a relative permittivity very close to unity are typically used to detect particles with momentum higher than 10 GeV/c (refs<sup>10–12</sup>).

The limitation of Cherenkov radiation in regular transparent dielectrics also comes from another reason: the total internal reflection at the air–dielectric interface will prevent the Cherenkov radiation generated by relativistic particles from being observed for relative permittivity  $\epsilon_r > 2$ , as coincidentally happens for most transparent dielectrics, and especially in the visible spectrum<sup>13</sup>. Having  $\epsilon_r > 2$  would lead to the existence of the

following inequality:  $\lim_{v \rightarrow c} \left( \frac{\epsilon_r \omega^2}{c^2} - \frac{\omega^2}{v^2} \right)^{1/2} > \frac{\omega}{c}$  for Cherenkov radiation

fields inside the dielectric, and then the fields outside the dielectric become evanescent. Besides, material losses (bulk absorption) have a large impact on the performance of Cherenkov detectors. Recently, anisotropic metal-based metamaterials with a complex permittivity, which still requires one component of the relative permittivity to be very close to one, have been proposed to control Cherenkov angles<sup>14</sup>. However, the existence of loss, which is particularly unavoidable in metal-based systems, will destroy the relation between the Cherenkov angle and the particle velocity, as described in Supplementary Section 4. Therefore, it will be necessary to use purely transparent systems to gain efficient control of the Cherenkov angle.

The studies of Cherenkov radiation and its applications have a long history<sup>3–6,15–19</sup>, and recently there has been renewed interest and progress in the topic<sup>20–29</sup>. However, the ability to control the Cherenkov angle in a flexible way is still limited by the permittivity of the radiator material as described above and remains very challenging.

Here, we propose a new underlying mechanism for the generation of Cherenkov radiation from a one-dimensional (1D) photonic crystal composed of widely available transparent dielectrics, which can transmit into air and thus can be used in Cherenkov detector designs such the ring-imaging Cherenkov detector. This comes from the constructive interference of the forward or backward resonance transition radiation from periodic dielectric interfaces. Therefore, along with the availability of many lossless dielectrics and the flexibility in the design of periodic structures<sup>30</sup>, this mechanism allows photonic crystals to flexibly control both the forward and backward Cherenkov angles. We note that while many phenomena based on Cherenkov radiation have been studied in photonic crystals<sup>22,27,31</sup>,

<sup>1</sup>State Key Laboratory of Modern Optical Instrumentation, The Electromagnetics Academy at Zhejiang University, Zhejiang University, Hangzhou, China.

<sup>2</sup>Division of Physics and Applied Physics, School of Physical and Mathematical Sciences, Nanyang Technological University, Singapore, Singapore.

<sup>3</sup>Particle Physics Department, Rutherford-Appleton Laboratory (STFC-UKRI), Didcot, UK. <sup>4</sup>Department of Physics, Massachusetts Institute of Technology, Cambridge, MA, USA. <sup>5</sup>Centre for Disruptive Photonic Technologies, NTU, Singapore, Singapore. <sup>6</sup>Department of Electrical Engineering, Technion-Israel Institute of Technology, Haifa, Israel. \*e-mail: [Sajan.Easo@cern.ch](mailto:Sajan.Easo@cern.ch)

including the backward (or reversed) Cherenkov radiation<sup>20</sup>, spectroscopy of photonic nanostructures<sup>3</sup>, and novel compact radiation sources<sup>4,17–19</sup>, the possibility of using photonic crystals to tailor the Cherenkov angle has not been directly addressed. In addition, the proposed Cherenkov detectors based on photonic crystals are different from transition radiation detectors<sup>32</sup>, where the latter relies only on the intensity of transition radiation from multilayer structures and disregards the information of radiation angles<sup>33–35</sup>.

To illustrate the underlying physics, we begin by schematically showing in Fig. 1 that the effective Cherenkov radiation can be generated by the constructive interference of resonance transition radiation excited from multiple interfaces in 1D photonic crystals. The simplest 1D photonic crystal can be constructed by alternating two different dielectric materials with relative permittivities denoted as  $\epsilon_{r1}$  and  $\epsilon_{r2}$  that are taken to be transparent (lossless); the impact of loss on the effective Cherenkov radiation from photonic crystals is described in Supplementary Section 6. When the relativistic particle with a charge of  $q$  and a velocity of  $\vec{v} = \hat{z}\beta c$  penetrates through a 1D photonic crystal, forward (backward) radiation can be generated in the bottom (top) air region, as shown in Fig. 1a. As a conceptual demonstration of resonance transition radiation, Fig. 1b presents the radiation field distribution (without the charge field) generated from a swift electron ( $\beta = 0.5022$ ) passing through a 1D photonic crystal ( $\epsilon_{r1} = 2$  and  $\epsilon_{r2} = 2.3$ ).

Resonance transition radiation from 1D photonic crystals is analytically calculated by extending Ginzburg and Frank's theory of transition radiation<sup>34,35</sup> to a 1D photonic crystal structure; the

detailed calculations are in Supplementary Sections 1–2. Since the particle velocity is below the Cherenkov threshold (that is,  $\beta < [\max(\epsilon_{r1}, \epsilon_{r2})]^{-1/2}$ ), there will be no conventional Cherenkov radiation within each dielectric. However, due to the transition radiation at each interface, plane-like waves are still emitted within the photonic crystal near the particle trajectory, as Fig. 1b clearly shows. Interestingly, the  $z$  component of Poynting's vector  $\mathbf{S}$  (which represents the direction of power flow) is antiparallel to the direction of motion of the particle. Consequently, more radiation energy enters into the top air region than into the bottom air region. These are characteristic features of the effective backward Cherenkov radiation, which originates entirely from the constructive interference of resonance transition radiation in the backward direction. This new mechanism for the generation of Cherenkov radiation is different from that of conventional Cherenkov radiation described by the theory developed by Frank and Tamm<sup>2,33</sup> and from that of Smith–Purcell radiation<sup>36,37</sup>. For the last two cases, the generated fields are directly emitted into the air region without the intermediate modulation by a periodic dielectric environment, and the charged particle moves only within one material without crossing interfaces between different materials.

We would like to emphasize that all of the radiation into air in the photonic crystal designs we propose comes only from the interference of resonance transition radiation. When the resonance transition radiation interferes constructively in air, it behaves similarly to the conventional Cherenkov radiation. In this sense, such resonance transition radiation can be treated as the effective

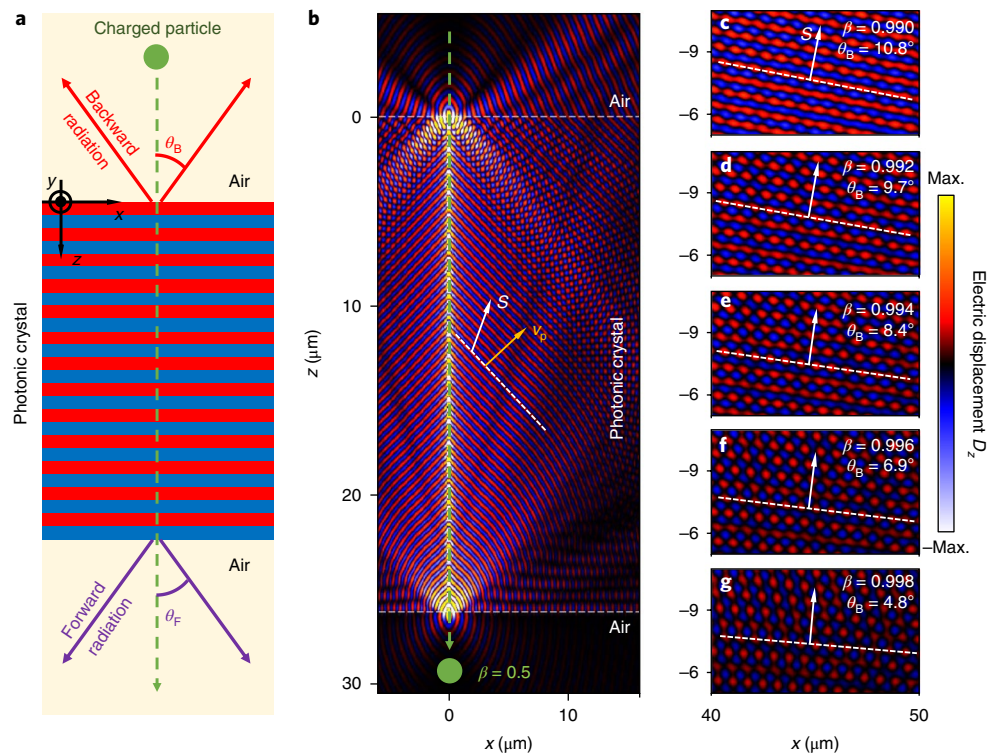


**Fig. 1 | Controlling Cherenkov angles with photonic crystals.** **a**, Structural schematic. The forward (backward) radiation is collected in the bottom (top) air region. **b–g**, Field distribution of backward Cherenkov radiation induced by the constructive interference of resonance transition radiation in the backward direction. In **b**, plane-like waves are excited near the particle trajectory (dashed green arrow), with the  $z$  components of both Poynting's vector  $\mathbf{S}$  and phase velocity  $\mathbf{v}_p$  being antiparallel to the direction of motion of the particle. In **c–g**, the Cherenkov angle is shown by the phase fronts of the far field in the top air region, exhibiting high sensitivity to the particle velocity  $v = \beta c$ . Here, and in the following figures, the working wavelength in air  $\lambda = 2\pi c/\omega$  is set to be 700 nm. In **b**, the photonic crystal consists of 40 unit cells; the thickness of the unit cell is  $d_{\text{unit}} = 0.9346\lambda$ ; within each unit cell, the thicknesses for the two dielectric constituents are  $d_1 = d_2 = 0.5d_{\text{unit}}$ ,  $\epsilon_{r1} = 2$  and  $\epsilon_{r2} = 2.3$ . In **c–g**, the thickness of the photonic crystal is 2 mm, with  $d_{\text{unit}} = 0.2792\lambda$ ,  $d_1 = 0.6d_{\text{unit}}$ ,  $d_2 = 0.4d_{\text{unit}}$ ,  $\epsilon_{r1} = 10.6$  and  $\epsilon_{r2} = 2.1$ .

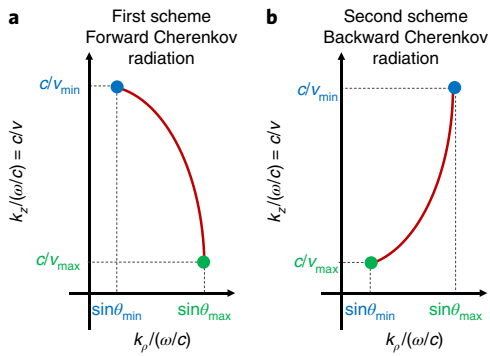


**Fig. 2 | Two conceptual schemes of controlling forward and backward Cherenkov angles with photonic crystals.** **a, b**, Hypothetical isofrequency contours of photonic crystals (that is, the relation between wavevectors  $k_\rho$  and  $k_z$ ) determine the relation between the Cherenkov angle in air,  $\theta = \text{asin}\left(\frac{k_z}{\omega/c}\right)$ , and the particle velocity,  $\frac{v}{c} = \frac{\omega/c}{k_\rho}$ . The goal of the two schemes is to create a wide range of Cherenkov angles for a narrow range of the particle velocity. In the first scheme (**a**), the maximum Cherenkov angle corresponds to the maximum particle velocity. In the second scheme (**b**), the maximum Cherenkov angle corresponds to the minimum particle velocity.

Cherenkov radiation of photonic crystal Bloch modes that can couple out to air, and whose phase velocity is smaller than the particle velocity; this is elaborated in Supplementary Section 6. In contrast, when the resonance transition radiation interferes destructively in air, it behaves similarly to the conventional transition radiation, and is devoid of the characteristic features of the Cherenkov radiation (because the corresponding Bloch modes that get emitted cannot couple out to air and are trapped inside the photonic crystal by total internal reflection). Importantly, the Cherenkov angles from photonic crystals can be sensitive to relativistic velocities of particles as illustrated in Fig. 1c–g.

The resonance transition radiation from 1D photonic crystals can be devised for manipulating the effective Cherenkov angles. To gain an intuitive understanding of such schemes, we qualitatively analyse the interaction between the charged particle and the eigenmodes of the photonic crystal. When the particle is assumed to move along the  $z$  direction, it induces a current density of  $\vec{J}^q(\vec{r}, t) = \frac{qv}{2\pi\rho} \delta(z-vt) \delta(\rho) \hat{z}$  in cylindrical coordinates<sup>34,35,38</sup>. By transforming all quantities to the frequency domain, we have the particle-induced fields proportional to  $\exp(i\frac{m}{v}z)$  (refs<sup>34,35,38</sup>), at each angular frequency  $\omega$ . From the momentum-matching condition, the charged particle is prone to excite the eigenmodes of photonic crystals with the wavevector along the  $z$  direction being  $k_z = \frac{c}{v} \frac{\omega}{c}$  (ref.<sup>17</sup>). Moreover, to guarantee that the excited modes inside the photonic crystal can reach the detectors (which are generally located in the air region—or more generally, in an external medium), we need to avoid the total internal reflection at the photonic crystal–air interface. This requires the wavevector along the  $\rho$  direction of the excited modes to be  $k_\rho \leq \frac{\omega}{c}$ . Due to the momentum matching along the  $\rho$  direction at the photonic crystal–air interface,  $k_\rho$  determines the Cherenkov angle  $\theta$  in the air region from the equation  $k_\rho = \frac{\omega}{c} \sin(\theta)$ .

From the above analysis, the relation between the Cherenkov angle in air and the particle velocity is effectively determined by the isofrequency contour of photonic crystals at each frequency (that is, the relation between the wavevectors  $k_z$  and  $k_\rho$ ). Two representative kinds of conceptual isofrequency contour of photonic crystals are shown in Fig. 2; practical examples of such contours can be seen in Supplementary Section 5. As the particle velocity increases in the range  $[v_{\min}, v_{\max}]$ , the Cherenkov angle in air increases in the range  $[\theta_{\min}, \theta_{\max}]$  in Fig. 2a, but decreases in the range  $[\theta_{\max}, \theta_{\min}]$  in Fig. 2b.

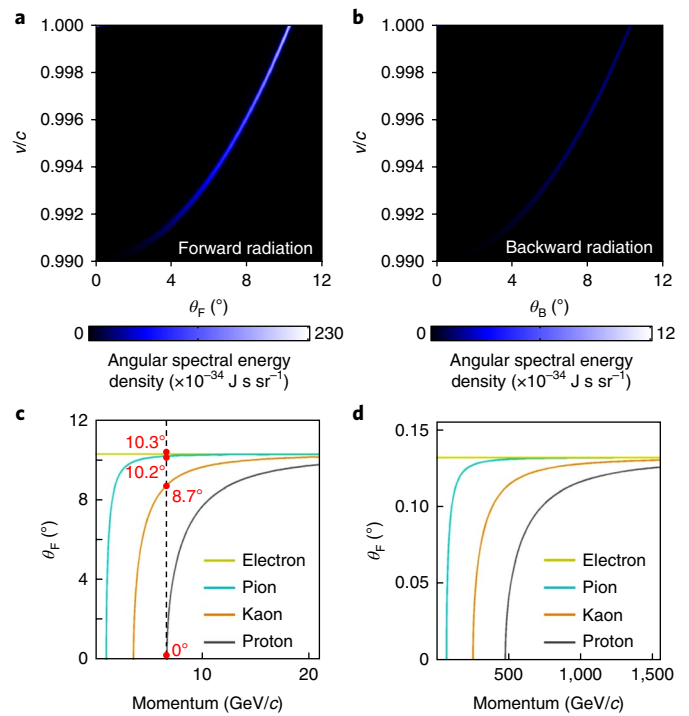


**Fig. 3 | Controlling Cherenkov angles with photonic crystals using the first scheme proposed.** **a, b**, Angular spectral energy density of forward (backward) radiation in the bottom (top) air region. The highly directional radiation in **a** shows the relation between the Cherenkov angle and the particle velocity. **c**, Cherenkov angles versus the particle momenta for four types of particle, where the velocity in **a** is converted to the momentum using the masses of the different particles. The thickness of the photonic crystal is 2 mm, with  $d_{\text{unit}} = 1.0205\lambda$ ,  $d_1 = 0.3d_{\text{unit}}$ ,  $d_2 = 0.7d_{\text{unit}}$ ,  $\epsilon_{r1} = 10.6$  and  $\epsilon_{r2} = 2.1$ . **d**, Cherenkov angles versus the particle momenta, where  $d_{\text{unit}} = 1.0144\lambda$  and the other parameters are the same as those in **c**. The results in this figure follow the proposed scheme in Fig. 2a.

Controlling Cherenkov angles using these two schemes in Fig. 2 are illustrated in Figs. 3 and 4. In these figures, the working wavelength in air is set to be 700 nm, and the relative permittivities of the two dielectric constituents of the photonic crystals configured are set to be  $\epsilon_{r1} = 10.6$  (such as GaP) and  $\epsilon_{r2} = 2.1$  (SiO<sub>2</sub>)<sup>13</sup>. Here, although the charge particles can create conventional Cherenkov radiation inside each dielectric layer, those photons remain trapped by total internal reflection at the dielectric–air interface and cannot contribute to radiation in the air. This is because the conventional Cherenkov radiation emerges with  $k_\rho = \frac{\omega}{c} \sqrt{\epsilon_r - \beta^2}$  (ref.<sup>33</sup>) that satisfies the condition of total internal reflection  $k_\rho > \frac{\omega}{c}$  (here  $\epsilon_r > 2$  and  $\beta \rightarrow 1$ ). In these figures, the forward (backward) angular spectral energy density  $U(\lambda, \theta) = \frac{dW}{d\omega d\Omega}$  (refs<sup>34,35,38</sup>), which represents the energy  $W$  radiated per unit angular frequency  $\omega$  per unit solid angle  $\Omega$  ( $d\Omega = 2\pi \sin\theta d\theta$ ), is adopted to characterize the forward (backward) radiation in the bottom (top) air region shown in Fig. 1 (more details are provided in Supplementary Section 3).

Figure 3 illustrates the first scheme of controlling Cherenkov angles as proposed in Fig. 2a. Figure 3a,b shows the angular spectral energy density from the photonic crystal. The resulting radiation energy in the air region flows predominantly along paths such that in each case the corresponding radiation angle is highly dependent on the particle velocity. Moreover, the forward radiation energy in Fig. 3a is  $\sim 100$  times larger than the backward radiation energy in Fig. 3b. Therefore, the resonance transition radiation from this photonic crystal can be effectively considered as the forward Cherenkov radiation. The weak backward radiation in Fig. 3b is attributed to

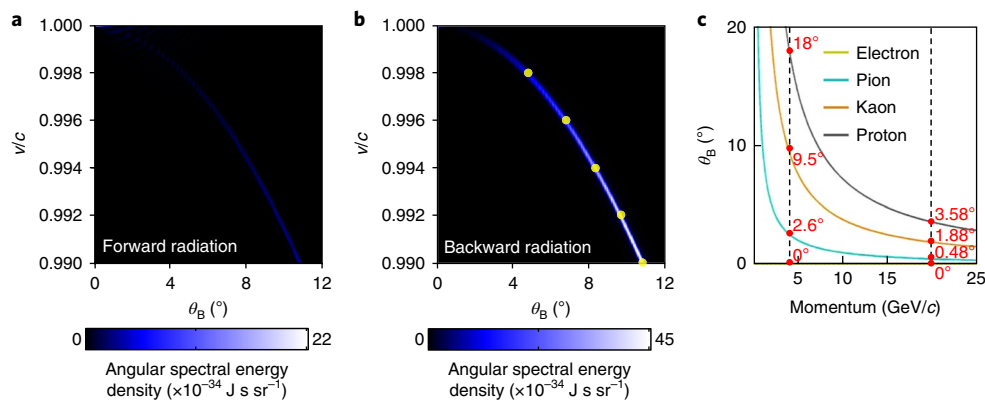


**Fig. 4 | Controlling Cherenkov angles with photonic crystals using the second scheme proposed.** **a, b**, Angular spectral energy density of forward (backward) radiation in the bottom (top) air region. The highly directional radiation in **b** shows the relation between the Cherenkov angle and the particle velocity. Cherenkov angles at five different particle velocities, denoted as yellow dots in **b**, are schematically shown by the far-field radiation in the top air region in Fig. 1c–g. **c**, Cherenkov angles versus the particle momenta for four kinds of particle, where the velocity in **b** is converted to the momentum using the masses of the different particles. The thickness of the photonic crystal is 2 mm, with  $d_{\text{unit}} = 0.2792\lambda$ ,  $d_1 = 0.6d_{\text{unit}}$ ,  $d_2 = 0.4d_{\text{unit}}$ ,  $\epsilon_{r1} = 10.6$  and  $\epsilon_{r2} = 2.1$ . The results in this figure follow the proposed scheme in Fig. 2b.

the mostly destructive interference of resonance transition radiation in the backward direction.

Although conventional transition radiation has no threshold for the particle velocity, the resonance transition radiation that constructively interferes in air has a threshold for the particle velocity  $v_{\text{threshold}}$  (as described in Supplementary Section 6.6), which in Fig. 3a is  $v_{\text{threshold}} = 0.99c$ . The appearance of such a threshold emphasizes the deep connection of this particular resonance transition radiation with the effective Cherenkov radiation of the Bloch modes. Altogether, the radiation into air can be classified into two regimes—that is, Cherenkov-like radiation when  $v > v_{\text{threshold}}$  and (non-resonance) transition-like radiation when  $v < v_{\text{threshold}}$ . These two categories of radiation can also be distinguished from their radiation spectra, as delineated in Supplementary Section 6.7. Here, for particle identification, we utilize the radiation with  $v > v_{\text{threshold}}$ .

The Cherenkov angle from photonic crystals is well suited for high-energy particle identification. For example, by applying the angle–velocity relation of Fig. 3a, we show the relation between the particle momentum and the Cherenkov angle for four types of particle in Fig. 3c. Here, for the hypothesis of the particle being an electron, a pion, a kaon or a proton with a momentum of 6.6 GeV/c, the corresponding Cherenkov angles are 10.3°, 10.2°, 8.7° or 0°, respectively. This would enable the different particle types to be effectively distinguished from one another in the region near this momentum. As another example, Fig. 3d shows the use of photonic crystals for particle identification at very high momenta ( $\sim 500$  GeV/c). It may also be noted that, as with conventional radiators, Cherenkov angles for all particle types in Fig. 3c,d tend to converge as the particles' momenta increase to large values (as described in Supplementary Section 6), thus requiring different photonic crystal designs for different momentum ranges.

Figure 4 shows the second scheme of controlling Cherenkov angles as proposed in Fig. 2b. The backward radiation energy in Fig. 4b is  $\sim 10$  times larger than the forward radiation energy in Fig. 4a. This is attributed to the constructive (destructive) interference of resonance transition radiation in the backward (forward) direction. Here also, the angular spectral energy density in air shows that the radiation angles are sensitive to the particle velocity. As a schematic demonstration of the effective backward Cherenkov radiation, the far-field distribution of radiation from an electron with different velocities highlighted by yellow dots in Fig. 4b is shown in Fig. 1c–g. Figure 4c shows the relation between the Cherenkov angles and the particle momenta for backward Cherenkov radiation

from photonic crystals. In this figure, for particles with a fixed momentum of 4 GeV/c (20 GeV/c), the Cherenkov angles corresponding to the electron, pion and proton hypothesis are 0°, 2.6°, 9.5° and 18° (0°, 0.48°, 1.88° and 3.58°), respectively. From this, one can infer that this scheme is also suitable for identification of high-energy particles and that it can be used in different momentum ranges.

These two schemes above help to surmount the limitations posed by conventional radiators. For example, to cover the momentum range 1–10 GeV/c, there is a dearth of suitable conventional materials with permittivity around 1.06. The silica aerogels<sup>12</sup> that are typically used for this suffer from significant losses due to Rayleigh scattering. To cover high momenta near 500 GeV/c would require using a gas at extremely low density and such a Cherenkov detector is difficult to operate.

While the forward Cherenkov radiation has been extensively studied<sup>9,10</sup>, the backward Cherenkov radiation<sup>39</sup> has never been considered for the design of Cherenkov detectors. When a photonic crystal is used for backward Cherenkov radiation in the second scheme, the emitted photon and the particle are naturally separated in opposite directions and hence their physical interference is minimized. This can lead to Cherenkov detector designs with two radiators for two different momentum ranges where the emitted photons go in forward or backward directions depending on the momentum of the charged particle. Such designs would reduce the hit occupancy in the corresponding photon detector planes and thus improve the particle identification performance, compared to the configuration where all of the photons go forward and reach a single-photon-detector plane. As another illustration, since the difference between the Cherenkov angles from an electron and a pion in Fig. 4c is much larger than that in Fig. 3c, the second scheme may offer a better precision in distinguishing between these particles than the first scheme and what is achievable from conventional radiators.

To facilitate the potential design of Cherenkov detectors based on photonic crystals, some of the salient features of the effective Cherenkov radiation from photonic crystals are described below. The number of photons emitted per unit length from the photonic crystal described in this paper is similar to that from anisotropic metamaterials in ref.<sup>14</sup>, but is one order of magnitude smaller than what could be achieved from an isotropic material of hypothetically similar refractive index as can be inferred from Fig. 3a and Supplementary Sections 3 and 4. One option to increase the photon yield is to increase the thickness of the crystal. Various options to

increase the yield are described in Supplementary Section 7. The fraction of the effective Cherenkov radiation emitted into the relevant direction is over 75% as shown in Supplementary Section 6.

The prospect of a thin photonic structure for the design of Cherenkov detectors is highly desirable because the gas radiators used for particle identification above 10 GeV/c are typically at least 1 m long. Using photonic crystals, the radiator length may be reduced to a few millimeters, considering that such crystals will have ~10,000 periods, with the potential to create a sufficient number of photons. The constraint in increasing the number of layers is that the amount of radiation energy loss introduced by the photonic crystal should be small enough to keep a low rate of secondary particle production. This would require using transparent dielectric materials made from combinations of materials with low atomic number such as silicon, oxygen, carbon and nitrogen. One also needs to ensure that the material used is radiation hard so that its properties do not degrade when used in a high-radiation environment such as the particle detector regions of the Large Hadron Collider.

We also note that using photonic crystals to design Cherenkov detectors might suffer from the chromatic aberration induced by the periodic structure. This also happens for Cherenkov detectors from anisotropic metal-based metamaterials<sup>14</sup>, due to the high-frequency dispersion of the permittivity in metals. The chromatic aberration will cause the Cherenkov angle to be sensitive to the frequency. Mitigating the chromatic effect is part of optimizing the photonic crystal design for a particular Cherenkov detector and some options for this are summarized below. They are described in more detail in Supplementary Section 6.

A simple option is to use filters to limit the frequency range, and to compensate for the corresponding reduction in photon yield, the number of layers may be increased. Another option is to limit the maximum momentum envisaged for particle identification from a given photonic crystal. For example, for the photonic crystal structure used in Fig. 3c, when the particle momentum is less than 3 GeV/c, the impact of chromatic aberration is negligible. A different approach is to measure the time of arrival of each photon on the detector plane to infer its wavelength and apply the required correction to the angle as described in ref.<sup>40</sup>. This method makes use of the variation in group velocity coming from the variation in wavelength of the photons produced.

A general approach, which minimizes the chromatic aberration inside the photonic crystal, is to use gain materials with anomalous dispersion<sup>41–43</sup> to construct the photonic crystal, since the material's anomalous dispersion can help to cancel the dispersion caused by the periodic structure. In Supplementary Section 6, this is elucidated with a numerical example for the 1–16 GeV/c range. The use of such gain materials may also help to augment the photon yield while keeping the radiator thin, since the photons emitted will be amplified during their propagation.

Alternatively, the use of optical elements (such as achromatic doublets) to apply such corrections, as done in many microscopes<sup>44,45</sup>, is also worth exploring. Moreover, the anisotropy in the crystal in the plane normal to the charged track direction may also help to magnify the Cherenkov angles produced<sup>14</sup> and thus reduce the effect of chromatic aberrations. After applying the correction to chromatic aberration using such approaches, the bandwidth can potentially be extended to over several tens to a few hundreds of nanometres, depending on the photonic crystal design and the dielectric materials used. The potential for such approaches is evinced with numerical examples in Supplementary Section 6.

It is also important to note that typical Cherenkov detectors receive particles along different trajectories. In experiments such as those at the Large Hadron Collider, several high-energy particles are produced in the region near the nominal interaction point of the beam particles, and then they move outward from that region. For

example, the particles produced in the pseudorapidity range from 2 to 5 (that is, travelling within a cone of about 300 mrad around the axis of collision) would be incident at small angles on a flat plane of the photonic crystal. For such cases, corrections can be applied to the above formalism<sup>34</sup> to estimate the Cherenkov angle. One can also design the photonic crystal such that it forms a spherical segment to facilitate normal incidence of a large fraction of such particles and thus minimize any such corrections. Since the radius of curvature of such a segment is much larger than the structural periodicity, we can consider the curved crystal as effectively a planar structure to a very good approximation. The fabrication of such a structure is different from that of conventional 1D photonic crystals. Nevertheless, a number of viable approaches already exist as indicated in Supplementary Section 7. These include multilayer polymer sheets (used as 1D photonic crystals in a number of applications<sup>46–48</sup>) that can be easily bent.

During the production of photonic crystals, one can deposit layers so that the required thickness of each layer can be attained with single-nanometre precision over large areas (tens of square centimetres and even square meters; for example, refs<sup>49,50</sup>). Some of the options available for this in the industry are described in Supplementary Section 7.

To conclude, this paper introduces a new mechanism (that is, the constructive interference of resonance transition radiation in the forward or backward direction) to generate Cherenkov radiation from a 1D photonic crystal. This new mechanism allows control of both the forward and backward Cherenkov angles in a flexible way, despite using transparent dielectrics with their relative permittivities far above unity, and thus overcomes the material limit for the design of conventional Cherenkov detectors. In particular, the Cherenkov angle from a photonic crystal can be engineered to be suitable for particle identification in very different momentum ranges, some of which cannot be achieved with conventional radiator materials. With the combined advantages of the abundant choice of dielectrics and the flexibility in the structural design, photonic crystals thus provide a new viable platform for the design of Cherenkov detectors with enhanced sensitivity and for the design of novel radiation sources.

## Methods

Methods, including statements of data availability and any associated accession codes and references, are available at <https://doi.org/10.1038/s41567-018-0138-4>.

Received: 19 September 2017; Accepted: 9 April 2018;

Published online: 14 May 2018

## References

- Cherenkov, P. A. Visible emission of clean liquids by action of gamma radiation. *Dokl. Akad. Nauk SSSR* **2**, 451–454 (1934).
- Frank, I. M. & Tamm, I. *Dokl. Akad. Nauk SSSR* **14**, 109–114 (1937).
- de Abajo, F. J. G. et al. Cherenkov effect as a probe of photonic nanostructures. *Phys. Rev. Lett.* **91**, 143902 (2003).
- Adamo, G. et al. Light well: A tunable free-electron light source on a chip. *Phys. Rev. Lett.* **103**, 113901 (2009).
- Cook, A. M. et al. Observation of narrow-band terahertz coherent Cherenkov radiation from a cylindrical dielectric-lined waveguide. *Phys. Rev. Lett.* **103**, 095003 (2009).
- Liu, F. et al. Integrated Cherenkov radiation emitter eliminating the electron velocity threshold. *Nat. Photon.* **11**, 289–292 (2017).
- Galbraith, W. & Jelley, J. V. Light pulses from the night sky associated with cosmic rays. *Nature* **171**, 349–350 (1953).
- Ypsilantis, T. & Seguinot, J. Theory of ring imaging Cherenkov counters. *Nucl. Instrum. Meth. A* **343**, 30–51 (1994).
- Adam, I. et al. The DIRC particle identification system for the BaBar experiment. *Nucl. Instrum. Meth. A* **538**, 281–357 (2005).
- Alves, A. A. Jr. et al. (LHCb Collaboration) The LHCb detector at the LHC. *J. Instrum.* **3**, S08005 (2008).
- Adinolfi, M. et al. (LHCb RICH Collaboration) Performance of the LHCb RICH at the LHC. *Eur. Phys. J. C* **73**, 2431 (2013).

12. Abashian, A. et al. The Belle detector. *Nucl. Instrum. Meth. A* **478**, 117–232 (2002).
13. Palik, E. D. *Handbook of Optical Constants of Solids*. (Academic, New York, NY, 1985).
14. Ginis, V., Danckaert, J., Veretennicoff, I. & Tassin, P. Controlling Cherenkov radiation with transformation-optical metamaterials. *Phys. Rev. Lett.* **113**, 167402 (2014).
15. Chamberlain, O., Segrè, E., Wiegand, C. & Ypsilantis, T. Observation of antiprotons. *Phys. Rev.* **100**, 947–950 (1955).
16. Aubert, J. J. et al. Experimental observation of a heavy particle. *J. Phys. Rev. Lett.* **33**, 1404–1406 (1974).
17. Liu, S. et al. Surface polariton Cherenkov light radiation source. *Phys. Rev. Lett.* **109**, 153902 (2012).
18. Wong, L. J., Kammer, I., Ilic, O., Joannopoulos, J. D. & Soljačić, M. Towards graphene plasmon-based free-electron infrared to X-ray sources. *Nat. Photon.* **10**, 46–52 (2016).
19. Denis, T. et al. Coherent Cherenkov radiation and laser oscillation in a photonic crystal. *Phys. Rev. A* **94**, 053852 (2016).
20. Luo, C., Ibanescu, M., Johnson, S. G. & Joannopoulos, J. D. Cherenkov radiation in photonic crystals. *Science* **299**, 368–371 (2003).
21. Xi, S. et al. Experimental verification of reversed Cherenkov radiation in left-handed metamaterials. *Phys. Rev. Lett.* **103**, 194801 (2009).
22. de Abajo, F. J. G. Optical excitations in electron microscopy. *Rev. Mod. Phys.* **82**, 209–275 (2010).
23. Vorobev, V. V. & Tyukhtin, A. V. Nondivergent Cherenkov radiation in a wire metamaterial. *Phys. Rev. Lett.* **108**, 184801 (2012).
24. Ren, H., Deng, X., Zheng, Y., An, N. & Chen, X. Nonlinear Cherenkov radiation in an anomalous dispersive medium. *Phys. Rev. Lett.* **108**, 223901 (2012).
25. Genevet, P. et al. Controlled steering of Cherenkov surface plasmon wakes with a one-dimensional metamaterial. *Nat. Nanotech.* **10**, 804–809 (2015).
26. Shi, X. et al. Caustic graphene plasmons with Kelvin angle. *Phys. Rev. B* **92**, 081404(R) (2015).
27. Kammer, I. et al. Quantum Čerenkov radiation: Spectral cutoffs and the role of spin and orbital angular momentum. *Phys. Rev. X* **6**, 011006 (2016).
28. Hummelt, J. S. et al. Coherent Cherenkov-cyclotron radiation excited by an electron beam in a metamaterial waveguide. *Phys. Rev. Lett.* **117**, 237701 (2016).
29. Duan, Z. et al. Observation of the reversed Cherenkov radiation. *Nat. Commun.* **8**, 14901 (2017).
30. Joannopoulos, J., Johnson, S., Winn, J. & Meade, R. *Photonic Crystals: Molding the Flow of Light* (Princeton Univ. Press, Princeton, NJ, 2011).
31. Zhang, Y. et al. Nonlinear Čerenkov radiation in nonlinear photonic crystal waveguides. *Phys. Rev. Lett.* **100**, 163904 (2008).
32. Andronic, A. & Wessels, J. P. Transition radiation detectors. *Nucl. Instrum. Meth. A* **666**, 130–147 (2012).
33. Jackson, J. D. *Classical Electrodynamics* (Wiley, Hoboken, NJ, 1999).
34. Ginzburg, V. L. & Tsytovich, V. N. *Transition Radiation and Transition Scattering* (CRC, Boca Raton, FL, 1990).
35. Ginzburg, V. L. & Tsytovich, V. N. Several problems of the theory of transition radiation and transition scattering. *Phys. Rep.* **49**, 1–89 (1979).
36. Smith, S. J. & Purcell, E. M. Visible light from localized surface charges moving across a grating. *Phys. Rev.* **92**, 1069 (1953).
37. Kammer, I. et al. Spectrally and spatially resolved Smith–Purcell radiation in plasmonic crystals with short-range disorder. *Phys. Rev. X* **7**, 011003 (2017).
38. Lin, X. et al. Splashing transients of 2D plasmons launched by swift electrons. *Sci. Adv.* **3**, e1601192 (2017).
39. Chen, H. & Chen, M. Flipping photons backward: reversed Cherenkov radiation. *Mater. Today* **14**, 34–41 (2011).
40. Dey, B. et al. Design and performance of the focusing DIRC detector. *Nucl. Instrum. Meth. A* **775**, 112–131 (2015).
41. Fang, A., Koschny, Th., Wegener, M. & Soukoulis, C. M. Self-consistent calculation of metamaterials with gain. *Phys. Rev. B* **79**, 241104(R) (2009).
42. Wuestner, S., Pusch, A., Tsakmakidis, K. L., Hamm, J. M. & Hess, O. Overcoming losses with gain in a negative refractive index metamaterial. *Phys. Rev. Lett.* **105**, 127401 (2010).
43. Wang, Y. T. et al. Gain-assisted hybrid-superlens hyperlens for nano imaging. *Opt. Exp.* **20**, 22953–22960 (2012).
44. Batson, P. E., Dellby, N. & Krivanek, O. L. Sub-ångstrom resolution using aberration corrected electron optics. *Nature* **418**, 617–620 (2002).
45. Kidger, M. J. *Fundamental Optical Design* (SPIE, Bellingham, WA, 2002).
46. Liu, R. Y. F. et al. Forced assembly of polymer nanolayers thinner than the interphase. *Macromolecules* **38**, 10721–10727 (2005).
47. Pursiainen, O. L. J. et al. Compact strain-sensitive flexible photonic crystals for sensors. *Appl. Phys. Lett.* **87**, 101902 (2005).
48. Arsenault, A. C., Puzzo, D. P., Manners, I. & Ozin, G. A. Photonic-crystal full-colour displays. *Nat. Photon.* **1**, 468–472 (2007).
49. Sheinflux, H. H. et al. Observation of Anderson localization in disordered nanophotonic structures. *Science* **356**, 953–956 (2017).
50. Shen, Y. et al. Optical broadband angular selectivity. *Science* **343**, 1499–1501 (2014).

## Acknowledgements

This work was sponsored by the National Natural Science Foundation of China (grants no. 61625502, 61574127 and 61601408), the ZJNSF (LY17F010008), the Top-Notch Young Talents Program of China, the Fundamental Research Funds for the Central Universities, the Innovation Joint Research Center for Cyber-Physical-Society System, Nanyang Technological University for NAP Start-Up Grant, the Singapore Ministry of Education (grants no. MOE2015-T2-1-070 and MOE2016-T3-1-006, and Tier 1 RG174/16 (S)) and the US Army Research Laboratory and the US Army Research Office through the Institute for Soldier Nanotechnologies (contract no. W911NF-18-2-0048 and W911NF-13-D-0001). I. Kammer is an Azrieli Fellow, supported by the Azrieli Foundation, and was partially supported by the Seventh Framework Programme of the European Research Council (FP7-Marie Curie IOF) under grant no. 328853-MC-BSiCS.

## Author contributions

X.L., I.K. and S.E. initiated the idea; X.L. performed the calculation; X.L., S.E., Y.S., H.C., B.Z., J.D.J., M.S. and I.K. analysed data, interpreted detailed results and contributed extensively to the writing of the manuscript; I.K., S.E., H.C., B.Z., J.D.J. and M.S. supervised the project.

## Competing interests

The authors declare no competing interests.

## Additional information

**Supplementary information** is available for this paper at <https://doi.org/10.1038/s41567-018-0138-4>.

**Reprints and permissions information** is available at [www.nature.com/reprints](http://www.nature.com/reprints).

**Correspondence and requests for materials** should be addressed to S.E.

**Publisher's note:** Springer Nature remains neutral with regard to jurisdictional claims in published maps and institutional affiliations.

## Methods

**Advantage of using photonic crystals to control Cherenkov radiation.** Using the two schemes described in the text, photonic crystals can control forward and backward Cherenkov angles, while conventional radiator materials, such as aerogels, gases or anisotropic metal-based metamaterials, can control only the forward Cherenkov angle<sup>9,10,14</sup>. Moreover, photonic crystals do not suffer from the strict limitations on the available values of dielectric permittivities, and instead overcome this material limit since they enable the use of transparent materials with arbitrary values of permittivity for the design of Cherenkov detectors.

**Derivation of resonance transition radiation.** Resonance transition radiation from 1D photonic crystals, which are composed of isotropic materials, is rigorously calculated by extending Ginzburg and Frank's theory of transition radiation within the framework of macroscopic electrodynamics. Since we mainly consider the case with  $\beta$  very close to 1, the high-energy particle can safely pass through the photonic crystal and its velocity is treated as constant.

In Supplementary Sections 1 and 2, an analytical expression of the radiated fields induced by a swift charged particle is obtained. By applying the Sommerfeld integration<sup>38</sup>, numerical calculation of the field distribution of resonance transition radiation is carried out as shown in Fig. 1.

Based on these radiation fields, the angular spectral energy densities of photons emitted in the top and bottom air regions shown in Fig. 1 are derived in Supplementary Section 3. The angular spectral energy density from an isotropic slab is shown in Supplementary Fig. 3 and that from a photonic crystal is shown in Figs. 3 and 4 and Supplementary Fig. 4. Since Maxwell equations are scalable, one can scale the wavelength by any factor and keep the same radiation characteristics (such as those in Figs. 3 and 4), as long as the structure of the photonic crystal scales by the same factor. We note that when the particle velocity increases, the radiation energy of the backward Cherenkov radiation decreases in Fig. 4b (see also Fig. 1c–g), while that of the forward Cherenkov radiation increases as in Fig. 3a.

The transition radiation from the interface between an isotropic material and a uniaxial material is also derived by using Ginzburg and Frank's theory of transition radiation. By following the principle of resonance transition radiation between isotropic materials, further derivation of the resonance transition radiation between uniaxial materials and the transition radiation from a uniaxial slab is carried out in Supplementary Section 4. The angular spectral energy density from a uniaxial slab is shown in Supplementary Fig. 5, where the influence of material losses on the relation between the Cherenkov angle and the particle velocity is discussed.

**Various features of Cherenkov radiation in our proposed photonic crystal designs.** Details are provided in Supplementary Section 6, including: the impact of local disorders in photonic crystals (Supplementary Section 6.1 and Supplementary Fig. 7), angular spread of Cherenkov radiation (Supplementary Section 6.2 and Supplementary Fig. 8) and momentum range for particle identification (Supplementary Section 6.3). The equivalence between the effective Cherenkov radiation into Bloch modes and the resonance transition radiation that constructively interferes in air is discussed in Supplementary Section 6.4. The radiation mechanism is further elaborated in Supplementary Section 6.5 and Supplementary Fig. 9, by presenting the phase velocity of the excited Bloch modes that can couple out to air.

Additional studies include the exploration of the velocity threshold in our mechanisms (Supplementary Section 6.6 and Supplementary Fig. 10), the similarity between radiation spectra from our photonic crystal designs and a dielectric slab (Supplementary Section 6.7 and Supplementary Figs. 11 and 12), the bandwidth and chromatic aberration correction of Cherenkov radiation from photonic crystals (Supplementary Section 6.8 and Supplementary Figs. 13–18), the angular spectral energy density and the angle-integrated radiation spectrum at a fixed velocity (Supplementary Section 6.9), the fraction of Cherenkov radiation emitted into the desired direction (Supplementary Section 6.10) and the impact of loss in material on our mechanism of Cherenkov radiation from photonic crystals (Supplementary Section 6.11 and Supplementary Fig. 19).

**Photonic crystals.** The band structure and isofrequency contour of the proposed 1D photonic crystal designs are calculated in Supplementary Section 5 (see Supplementary Fig. 6).

**Production and use of photonic crystals in high energy physics experiments.** Details are provided in Supplementary Section 7. This section includes the references to the various methods available in the industry for the production of large-area photonic crystals and flexible photonic crystals (Supplementary Section 7.1) and the options to increase the photon yield obtained from photonic crystals (Supplementary Section 7.2).

**Data availability.** The data that support the plots within this paper and other findings of this study are available from the corresponding author upon reasonable request.